Tribology International 93 (2016) 182–189

Contents lists available at ScienceDirect

Tribology International

journal homepage: www.elsevier.com/locate/triboint

A role of friction-induced torque in sliding friction of rubber materials

Satoru Maegawa*, Fumihiro Itoigawa, Takashi Nakamura

Department of Mechanical Engineering, Nagoya Institute of Technology, Gokiso-cho Showa-ku, Nagoya, Aichi 466-8555, Japan

ARTICLE INFO

Article history:
Received 27 June 2015
Received in revised form
4 August 2015
Accepted 15 August 2015
Available online 24 August 2015

Keywords:
Rubber
Friction force
Friction-induced torque
Real contact area

ABSTRACT

Herein, the role of friction-induced torque in sliding friction of rubber materials is investigated. A friction tester was developed to monitor the friction force between a silicon rubber block and a surface made of PMMA[1]. Based on the experimental results, a simplified model was developed to express the nonuniform distribution of normal pressure developed due to the friction-induced torque, and the normal pressure dependence of the real contact area based on Persson's contact theory. Based on the modeling, the mechanism of the effect of the friction-induced torque on frictional force reductions was clarified.

1. Introduction

Understanding the mechanism of interfacial friction is a major and an interesting topic in the field of mechanical engineering. The frictional behavior of a contact interface determines the abilities of the sliding system, such as the accuracy of positioning, sliding stability, system stiffness, and damping properties. However, it is difficult to predict frictional behaviors in advance, at the design stage, because friction force depends on a number of factors, such as, material, lubricant, surface topography, operating condition, mechanical property of sliding systems, and other environmental conditions [1–3].

Friction-induced torque is an important factor for the determination of the frictional behavior of sliding systems [4,5]. In most sliding systems a torque results from an interfacial friction force and the applied tangential load. This is because the tangential load is not applied exactly in the plane of the sliding interface. The torque causes a nonuniform spatial distribution of the normal contact pressure, and it strongly affects the value of the friction force.

Scheibert and Dysthe [4] discussed the effect of frictional-induced torque on stick-slip motion using a minimal dualistic model, in which an elastic block slides on a rigid smooth plane with a friction-induced torque that arises from an external tangential load and a frictional force. In this analysis, they explained that the increase in friction-induced torque enhanced the occurrence of microslip nucleation, namely the precursors, and it reduced the value of the static friction. Thus, this study theoretically declared that the static friction depends on the shape of the slider. As pointed out by David and Lorenz [6,7], "static friction coefficient is a not material constant".

When a rubber slider slides on a rigid smooth plane, friction forces (not only static friction but also kinetic friction) are significantly influenced by the magnitude of the friction-induced torque. For example, Murarash [8] developed a new concept where the kinetic friction force can be controlled by the positive use of the deformation of hexagonal pillars fabricated on the contact interface. The density number and the aspect ratio of the pillars are important factors for determining friction force. Similar approaches, focusing on the positive use of the deformation of the surface patterns, have also been utilized by other researchers [9,10].

In this study, we focused on the effect of the deformation of a rubber slider on the friction coefficient due to the friction-induced torque. A friction tester, in association with a total reflection optical system, was developed to directly observe the sliding interface between a silicon rubber block and a smooth plane made of poly(methyl methacrylate) (PMMA). From measurements of the friction force and observations of the contact interface, it was found that the shape of the rubber slider is an important factor for the determination of friction forces. When a rubber slider with a large height and a small length was used, a highly nonuniform distribution of the real contact area was observed within the apparent contact region. In this case, a relatively small friction force was obtained, compared to that of a slider with a small

* Corresponding author. Tel.: +81 52 735 54; fax: +81 52 735 5429.
E-mail address: maegawa.satoru@nitech.ac.jp (S. Maegawa).

[1] PMMA: poly(methyl methacrylate).

http://dx.doi.org/10.1016/j.triboint.2015.08.030
0301-679X/

height and a large length. Furthermore, in order to discuss the mechanism of the dependence of the friction coefficient on the shape of the slider, a simplified friction model was developed. The model can express the effect of the friction-induced torque on the spatial distribution of the normal contact pressure. Based on Persson's contact theory [11,12], the normal pressure dependence of the real contact area is also expressed. Consequently, it was found that the existence of the friction-induced torque reduces the total real contact area, leading to a decreased friction force.

2. Materials and methods

2.1. Apparatus

Fig. 1 shows the schematic of the experimental apparatus. The apparatus employs a contact interface between the bottom face of a silicon rubber block and the upper face of a transparent dove prism made of PMMA. The rubber slider was fixed under an X-directional stage via a lever system. The dove prism was fixed on a dynamometer using a steel folder. As illustrated in the side view of the apparatus, Fig. 1(b), a total reflection optical system was provided to directly observe a sliding interface between the rubber block and the PMMA prism. The optical system consists of a light emitting diode (LED) light source, the dove prism, a lens tube system, and a CCD camera. To achieve a total reflection at noncontact regions, the incident angle to the contact interface was set to 60°, and was larger than the critical angle necessary for the total reflection at the interface between PMMA and air (42°). Thus, an incident light that illuminates a noncontact region is perfectly reflected at the PMMA-air interface [13–15]. In contrast, in real contact regions, an incident light beam propagates without the total reflection; the light was absorbed or scattered. Therefore, we can visualize the spatial distribution of the real contact regions by capturing the spatial distribution of the reflected light.

2.2. Specimens

Several types of different slider blocks made of silicon rubber (Shore A 70) were used. The geometry of these blocks is listed in Fig. 2. The bottom face of the blocks was polished by a sand paper. The power spectrum of the bottom surface of a rubber block is also shown in the right side of the figure.

2.3. Procedure

First, using the lever mechanics with a dead weight of 30 N (see Fig. 1) the normal load was applied on the contact interface. In order to neglect the effect of the contact time on the total real contact area [16,17], sliding tests were then performed after a wait time of 200 s.

Subsequently, the X stage started to move at a constant speed of 0.1 mm/s. During the sliding motion, normal and tangential loads, i.e., F_X and F_Z, were monitored with the dynamometer and data logger at a sampling rate of 1 kHz. Additionally, the spatial distribution of the reflected light from the contact interface was captured by the CCD camera before the sliding test and during steady sliding motion. This sequence was repeated 5 times for each specimen.

The resolutions of the optical system along the X and Y directions were 30 and 140 μm, respectively. As previously pointed out [18], the measured quantity of the real contact area strongly depends on the resolution (or magnification) of the optical systems used. Thus, we should take into account the effect of the optical resolution on the measured real contact area.

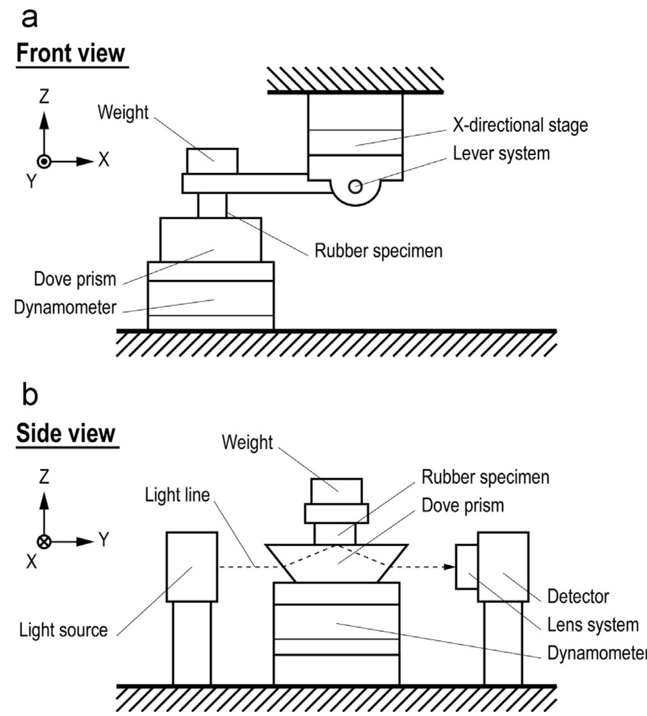

Fig. 1. A schematic of the experimental apparatus: (a) front view and (b) side view.

3. Results

3.1. Temporal changes of tangential loads

Fig. 3 shows the temporal changes in the tangential load F_X for $L = 10$ mm, i.e., specimens A, B, C, D and E. The origin of the abscissa is the time when the X stage starts to move along the X direction. From the figure, it was found that the tendency of temporal changes in F_X strongly depended on the height of specimen H. The labels that describe the type of the specimen are arranged from the bottom up in an increasing order of the friction force value. Thus, the friction force of specimen A has the largest value. In contrast, the frictional force of specimen E has the smallest value.

As a general feature, it was found that temporal changes in F_X are divided into two stages. In the first stage, F_X gradually increased until it reaches a maximum value, i.e., the maximum static friction, F_{smax}. The magnitude of the slope of F_X is dependent on the height of the slider, because the compliance of the slider is characterized by its shape. Subsequently, in the second stage, F_X approached a steady value, i.e., the value of the kinetic friction force F_k. Similar to the case of the magnitude of the slope, the value of F_k also depended on the slider.

Fig. 4 summarizes the effects of the height H and length L of the slider on the friction coefficient μ, where μ is determined as the ratio of the kinetic friction force F_k on the normal load F_Z, i.e., $\mu = F_k/F_Z$. It is clear that the value of μ decreases with increasing H values. In contrast, μ increases with L. The three solid lines are fitted by the least-squares method. The magnitude of the slope at $L = 20$ mm was -0.0032, that at $L = 15$ mm was -0.0057, and that at $L = 10$ mm was -0.014. Thus, the absolute value of the slope increased with decreasing L.

3.2. Spatial distribution of real contact area

To visualize the spatial distribution of the real contact area within the apparent contact region, the intensity map of the